Supporting Information

Phonon-Assisted Exciton Transfer into Silicon Using Nanoemitters: The Role of Phonons and Temperature Effects in Förster Resonance Energy Transfer

Aydan Yeltik [1‡], Burak Guzelturk [1‡], Pedro Ludwig Hernandez-Martinez [1 2], Alexander O. Govorov[3], and Hilmi Volkan Demir[1 2]

[1] Department of Electrical and Electronics Engineering, Department of Physics, UNAM - Institute of Materials Science and Nanotechnology, Bilkent University, Ankara 06800 Turkey

[2] School of Electrical and Electronic Engineering, School of Physical and Mathematical Sciences, Nanyang Technological University, Nanyang Avenue, Singapore 639798, Singapore

[3] Clippinger Research Labs, Department of Physics and Astronomy, Ohio University, Athens OH 45701 USA

‡ These authors contributed equally to this work

A. Model of phonon-assisted FRET from CdSe/ZnS QDs to monocrystalline bulk silicon

In this study, we used the Fermi's Golden rule as the starting point to construct our FRET model. To begin with, we discuss the basic features of the FRET model; the probability of an exciton transfer from a donor nanostructure to an acceptor nanostructure is given by the

Fermi's Golden rule

$$\gamma_{NRET} = \frac{2}{\hbar}\left\{\sum_{f}\left|\left\langle f_{exc};0_{exc}\left|\hat{V}_{\text{int}}\right|i_{exc};0_{exc}\right\rangle\right|^{2}\delta\left(\hbar\omega_{exc}-\hbar\omega_{f}\right)\right\}\ ,$$

(S1)

where $\left|i_{exc};0_{exc}\right\rangle$ is the initial state with an exciton in the donor and zero exciton in the acceptor; $\left|f_{exc};0_{exc}\right\rangle$ is the final state with an exciton in the acceptor and zero exciton in the donor; $\hat{V}_{\text{int}}$ is the exciton Coulomb interaction operator; and $\hbar\omega_{exc}$ is the exciton's energy. Neglecting the coherent coupling between excitons, i.e., the initial and final states can be written as $\left|i_{exc};0_{exc}\right\rangle = \left|i_{exc}\right\rangle\left|0_{exc}\right\rangle$ and $\left|f_{exc};0_{exc}\right\rangle = \left|f_{exc}\right\rangle\left|0_{exc}\right\rangle$, and using the fluctuation dissipation theorem (FDT)[1] together with the QD formalism developed in Refs. [2,3], the Fermi's Golden rule can be simplified as

$$\gamma_{NRET} = \frac{2}{\hbar}\text{Im}\left[\int dV\left(\frac{\varepsilon_{A}(\omega)}{4\pi}\right)\mathbf{E}_{in}(\mathbf{r})\cdot\mathbf{E}_{in}^{*}(\mathbf{r})\right]$$

(S2)

where $\mathbf{E}_{in}(\mathbf{r})$ includes the effective electric field created by an exciton in the donor.

Here, the electric field is calculated with

$$\mathbf{E}(\mathbf{r}) = -\nabla\Phi(\mathbf{r})$$

(S3)

The electric potential, $\Phi(\mathbf{r})$, needed to compute γ_{NRET} (Eq. S1) should be calculated as a total potential created by the electric potential of an exciton (in the donor side)

$$\Phi_\alpha(\mathbf{r}) = \left(\frac{ed_{exc}}{\varepsilon_{eff_D}}\right)\frac{(\mathbf{r}-\mathbf{r}_0)\cdot\hat{\boldsymbol{\alpha}}}{|\mathbf{r}-\mathbf{r}_0|^3} \tag{S4}$$

where ed_{exc} is the dipole moment of the exciton and ε_{eff_D} is the effective dielectric constant of the donor, which depends on the geometry and the exciton dipole direction, $\alpha = x, y, z$.

The average FRET rate is calculated as

$$\gamma_{NRET} = \frac{\gamma_{x,NRET} + \gamma_{y,NRET} + \gamma_{z,NRET}}{3} \tag{S5}$$

where $\gamma_{\alpha,NRET}$ is the transfer rate for the α-exciton ($\alpha = x, y, z$). For a spherical QD, the corresponding transfer rates are

$$\gamma_{\alpha,NRET}(d,\omega_{exc}) = \frac{2}{\hbar}b_\alpha\left(\frac{ed_{exc}}{\varepsilon_{eff}}\right)^2\frac{1}{d^3}\left|\frac{2\varepsilon_0}{\varepsilon_{si}(\omega_{exc})+\varepsilon_0}\right|^2 \mathrm{Im}\left[\varepsilon_{si}(\omega_{exc})\right] \tag{S6}$$

where ε_0 is the medium dielectric constant, $\varepsilon_{eff} = \frac{2\varepsilon_0+\varepsilon_{QD}}{3}$ is the effective dielectric constant, ε_{QD} is the QD dielectric constant, $\varepsilon_{Si}(\omega)$ is the silicon dielectric function (taking from Ref. [4]), and $b_\alpha = \frac{1}{8}, \frac{1}{16}, \frac{1}{16}$ for an exciton *x*, *y*, and *z*, respectively. Thus the total FRET rate is

$$\gamma_{NRET}(d,\omega_{exc}) = \frac{2}{\hbar}\left(\frac{1}{12}\right)\left(\frac{ed_{exc}}{\varepsilon_{eff}}\right)^2\frac{1}{d^3}\left|\frac{2\varepsilon_0}{\varepsilon_{si}(\omega_{exc})+\varepsilon_0}\right|^2 \mathrm{Im}\left[\varepsilon_{si}(\omega_{exc})\right] \tag{S7}$$

Eq. S7 describes the energy transfer from a QD to a bulk semiconductor material. In this study, the FRET rates are investigated using a hybrid structure consisting of 10-monolayer-equivalent QD film on bulk silicon as proposed in the letter. For simplicity, the excitation energy transfer from a monolayer of the QDs to bulk silicon is considered as the energy transfer from a single QD in the same layer to the silicon, and it is attributed to the average energy transfer. To find the lifetimes of the QDs, the FRET rate of the QDs, $\langle \gamma_{NP} \rangle = 1/\tau_{NP}$, was formulated as

$$\left\langle \gamma_{NP}\left(d,\omega,T\right)\right\rangle = \gamma_0\left(d,\omega,T\right) + \frac{1}{N}\sum_{i=1}^{N}\gamma_{i,NRET}\left(d_i,\omega\right) \tag{S8}$$

where $\gamma_0\left(d,\omega,T\right) = \frac{1}{\tau_0(d,\omega,T)}$ is the QD exciton recombination rate in the absence of silicon; τ_0 is the QD exciton lifetime in the absence of silicon; $\gamma_{i,NRET}\left(d_i,\omega\right)$ energy transfer for a QD in the *i-th* layer; and *N* is the total number of QD layers. Since silicon is an indirect bandgap semiconductor, we included its temperature-dependent parameters into the model, which provides us with a phonon-assisted FRET model as shown in Eq. S9.

$$\gamma_{NRET}\left(d,\omega_{exc},T\right) = \frac{2}{\hbar}\left(\frac{1}{12}\right)\left(\frac{ed_{exc}}{\varepsilon_{eff}}\right)^2 \frac{1}{d^3}\left|\frac{2\varepsilon_0}{\varepsilon_{si}\left(\omega_{exc},T\right)+\varepsilon_0}\right|^2 \mathrm{Im}\left[\varepsilon_{si}\left(\omega_{exc},T\right)\right] \tag{S9}$$

Eq. S9 gives the energy transfer rate for two point-like dipoles, i.e., a perfect donor and acceptor pair. To include the energy transfer losses for the QDs due to imperfections, traps,

etc. (i.e., nonradiative channels not included in our derivation) as a function of temperature, we introduced the factor $\frac{Y_{QD}(T)\gamma_0^D(T)}{Y_{QD}\gamma_0^D(T_{Room})}$ from the QY definition. Thus, Eq. S9 was modified as

$$\gamma_{NRET}\left(d,\omega_{exc},T\right)=\left(\frac{Y_{QD}\left(T\right)\gamma_0^D\left(T\right)}{Y_{QD}\left(T_{Room}\right)\gamma_0^D\left(T_{Room}\right)}\right)\frac{2}{\hbar}\left(\frac{1}{12}\right)\left(\frac{ed_{exc}}{\varepsilon_{eff}}\right)^2\frac{1}{d^3}\left|\frac{2\varepsilon_0}{\varepsilon_{si}\left(\omega_{exc},T\right)+\varepsilon_0}\right|^2\mathrm{Im}\left[\varepsilon_{si}\left(\omega_{exc},T\right)\right] \quad \textbf{(S10)}$$

Eq. S10 models the energy transfer rate as a function of temperature and exciton energy. As observed from Figure S0, as compared to the efficiency of FRET from QDs into silicon (3D) with the efficiencies for acceptors having various dimensions (2D, 1D and 0D: distance dependencies of d^{-4}, d^{-5} and d^{-6}, respectively), the FRET efficiencies are still preserved at a distance more than 30 nm corresponding to more than first four monolayers in the film owing to the d^{-3} distance dependence.

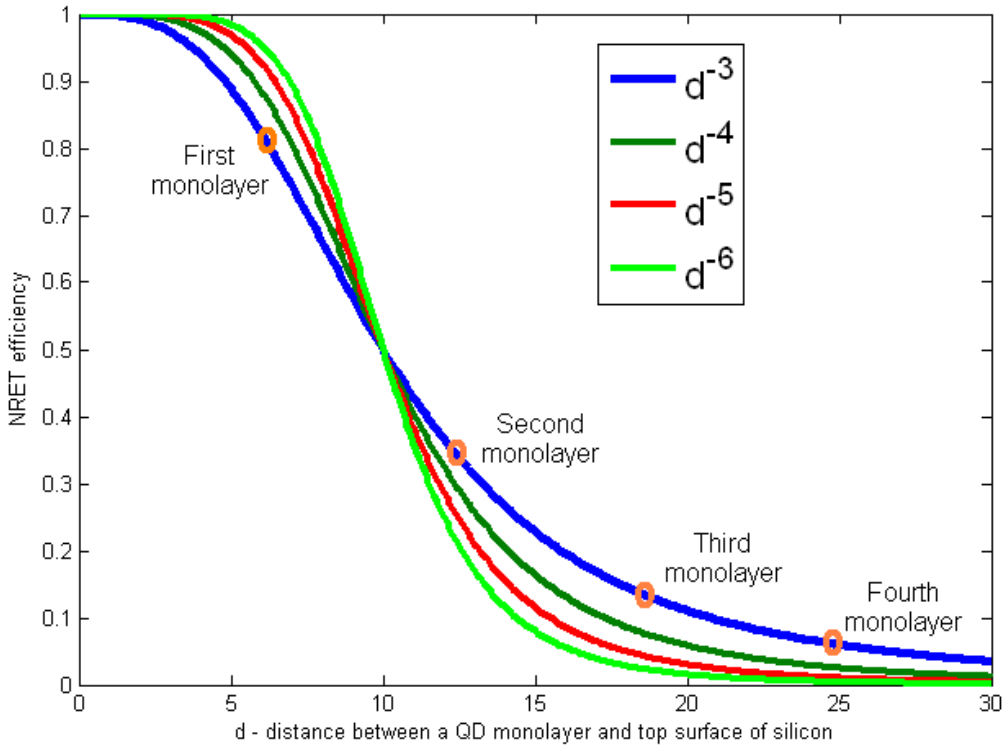

Figure S0. FRET efficiencies are plotted as a function of separation of a QD monolayer to the top surface of silicon. FRET efficiencies of the consecutive QD monolayers are marked on the plot.

The model ("phonon assisted") is extended to include temperature-dependent silicon dielectric function which is directly related to the phonon assisted optical properties of silicon. Furthermore, temperature-dependent QYs of the donor QDs are considered in the modified model ("Full temperature-dependent"). This allowed us to correctly account for the radiative decay part of the QDs as a function of temperature which is important to calculate the dipole-dipole coupling. With these modifications, the phonon-assisted FRET model fitted better to the TRF lifetimes, as it is shown in the study.

B. Correction for the radiative lifetime of QDs due to the refractive index difference in the substrate

The correction factor due to the difference in refractive index of substrate material for our QD-sapphire hybrid system is estimated using the assumptions and conditions given in ref. 5 (section 10.5 equation 10.26) and averaged over random dipole orientations.[6] The dipole decay rate, located at distance *z* above a layered dielectric system, is modified from γ_0 to γ, where γ_0 is the dipole decay rate in vacuum. The ratio between these two rates is given by

$$\frac{\gamma}{\gamma_0} = 1 + I\left(0,\infty\right)$$

(S11)

$$I\left(a,b\right) = \frac{1}{2}\mathrm{Re}\left(\int_a^b \frac{sds}{\sqrt{1-s^2}}\left[\left(2s^2-1\right)r^{(p)}\left(s\right)+r^{(s)}\left(s\right)\right]\exp\left[2ik_0\left(\sqrt{1-s^2}\right)h\right]\right)$$

(S12)

where $r^{(s)}\left(s\right)$ and $r^{(p)}\left(s\right)$ are the reflection coefficients for s- and p-polarized waves (Ref. [19] in the main text), respectively, defined as

$$r^{(s)}\left(s\right) = \frac{r_{1,2}^{(s)}\left(s\right)+r_{2,3}^{(s)}\left(s\right)\exp\left[2i\left(\sqrt{k_2^2-s^2k_1^2}\right)z\right]}{1+r_{1,2}^{(s)}\left(s\right)r_{2,3}^{(s)}\left(s\right)\exp\left[2i\left(\sqrt{k_2^2-s^2k_1^2}\right)z\right]}$$

(S13)

$$r^{(p)}\left(s\right) = \frac{r_{1,2}^{(p)}\left(s\right)+r_{2,3}^{(p)}\left(s\right)\exp\left[2i\left(\sqrt{k_2^2-s^2k_1^2}\right)z\right]}{1+r_{1,2}^{(p)}\left(s\right)r_{2,3}^{(p)}\left(s\right)\exp\left[2i\left(\sqrt{k_2^2-s^2k_1^2}\right)z\right]}$$

(S14)

with

$$r_{1,2}^{(s)}(s)=\frac{k_1\sqrt{1-s^2}-\sqrt{k_2^2-s^2k_1^2}}{k_1\sqrt{1-s^2}+\sqrt{k_2^2-s^2k_1^2}}$$

(S15)

$$r_{2,3}^{(s)}(s)=\frac{\sqrt{k_2^2-s^2k_1^2}-\sqrt{k_3^2-s^2k_1^2}}{\sqrt{k_2^2-s^2k_1^2}+\sqrt{k_3^2-s^2k_1^2}}$$

(S16)

$$r_{1,2}^{(p)}(s)=\frac{\varepsilon_2k_1\sqrt{1-s^2}-\varepsilon_1\sqrt{k_2^2-s^2k_1^2}}{\varepsilon_2k_1\sqrt{1-s^2}+\varepsilon_1\sqrt{k_2^2-s^2k_1^2}}$$

(S17)

$$r_{2,3}^{(p)}(s)=\frac{\varepsilon_3\sqrt{k_2^2-s^2k_1^2}-\varepsilon_2\sqrt{k_3^2-s^2k_1^2}}{\varepsilon_3\sqrt{k_2^2-s^2k_1^2}+\varepsilon_2\sqrt{k_3^2-s^2k_1^2}}$$

(S18)

$$s=\frac{\sqrt{{k_{ix}}^2+{k_{iy}}^2}}{k_i}=k_i\sin(\theta)/k_i$$

here ε_i and k_i $(i=1,2,3)$ are the dielectric constant and wave vector of the medium 1, 2 and 3 as depicted in Figure S1.

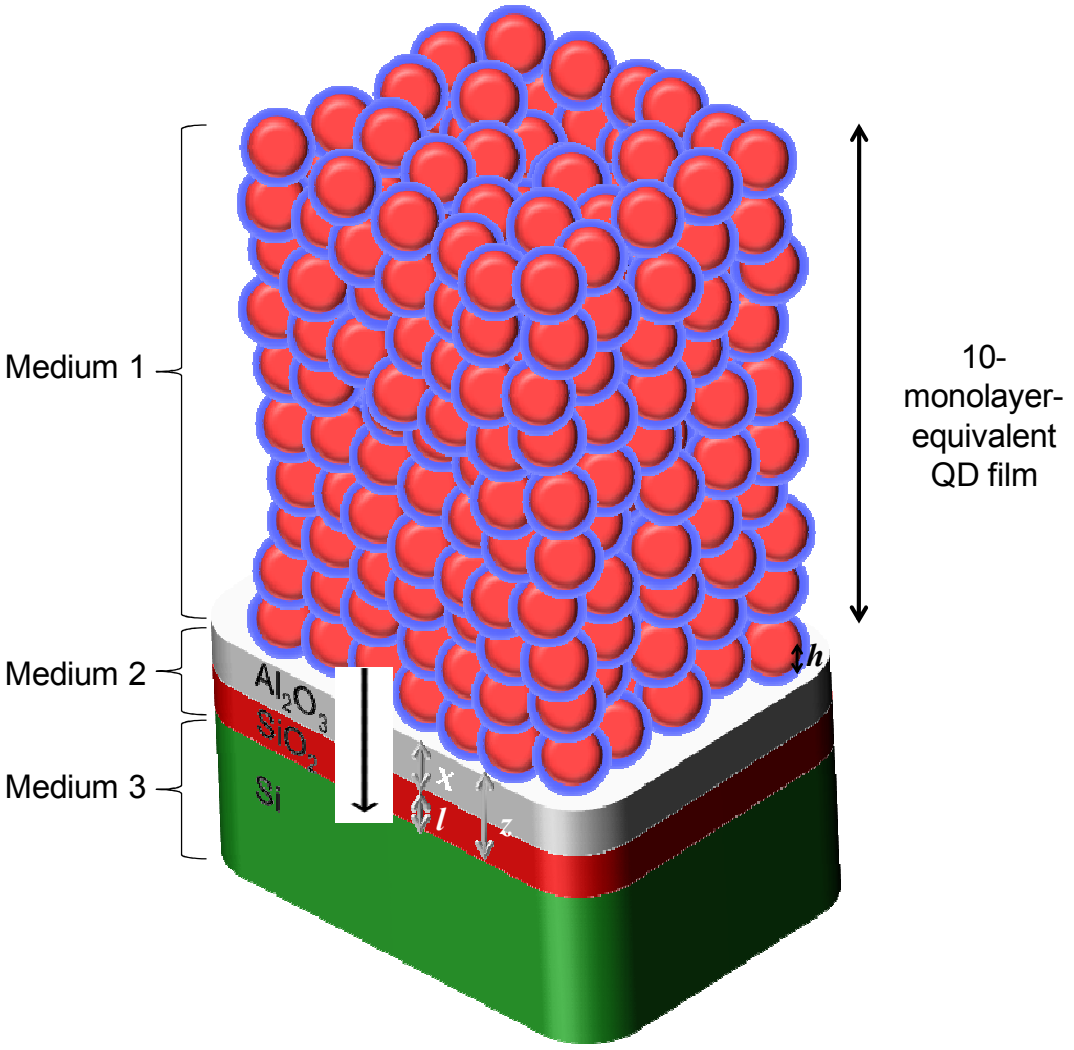

Figure S1. Here, z is the dielectric thickness of the effective oxide layer on silicon, h is the distance between the dipole and the topmost dielectric layer, $l = 1.65$ nm is the SiO_2 film thickness, X ranging from 0 to 4.0 nm is the Al_2O_3 film thickness and d is the distance from a QD monolayer center of interest to the bulk silicon.

In a QD the exciton recombination rate is

$$\gamma^{QD} = \gamma_r^{QD} + \gamma_{nr}^{QD}$$

(S19)

The average recombination rate for 10-monolayer-equivalent QD film (ignoring QD-QD FRET) can be written as

$$\left\langle \gamma^{QD} \right\rangle = \frac{1}{N}\sum_{i=1}^{N} \gamma_i^{QD}$$

(S20)

However, the QD recombination rate changes when a QD is placed in close proximity to a dielectric layer because of the inhomogeneity of the dielectric constants. This alters the radiative recombination rates, while nonradiative part remains unchanged $\gamma_{nr}^{QD} = \gamma_{0,nr}^{QD}$. This change in radiative part is expressed for QDs on Si and Al_2O_3 as follows

$$\gamma_{Al_2O_3,r}^{QD} = \alpha^{Al_2O_3}\gamma_{0,r}^{QD}$$

(S21)

$$\gamma_{Si,r}^{QD} = \alpha^{Si}\gamma_{0,r}^{QD}$$

(S22)

where

$$\alpha^{Al_2O_3} = \frac{1}{N}\left(\sum_{i=1}^{N} \alpha_i^{Al_2O_3}\right)$$

(S23)

$$\alpha^{Si} = \frac{1}{N}\left(\sum_{i=1}^{N} \alpha_i^{Si}\right)$$

(S24)

$\gamma_{0,r}^{QD}$ $\gamma_{Al_2O_3,r}^{QD}$ $\gamma_{Si,r}^{QD}$ are the radiative recombination rates in vacuum, on Al_2O_3 and Si, respectively. Here, α_i is the factor, which relates the modification of radiative lifetimes with respect to vacuum, calculated for the i-th QD monolayer using Eqn S11 and averaged for all QD monolayers on Al_2O_3 and Si denoted as $\alpha^{Al_2O_3}$ and α^{Si}, respectively. We took the integral in Eqn S12 from 0 to 4 in order to correct the radiative part including the effects of the QDs' intrinsic radiative recombination and RET from the QDs into silicon.

To account for the effect of refractive index difference between Al_2O_3 and Si on the radiative lifetime of QDs, we calculate a correction factor α using the expression

$$\alpha = \frac{\gamma_{Si,r}^{QD}}{\gamma_{Al_2O_3,r}^{QD}} = \frac{\alpha^{Si}}{\alpha^{Al_2O_3}} \tag{S25}$$

On Al_2O_3 radiative and nonradiative recombination rates are written in terms of quantum yields (Y_{QD}) as $\gamma_{Al_2O_3,r}^{QD} = Y_{QD}\gamma_{Al_2O_3}^{QD}$ and $\gamma_{Al_2O_3,nr}^{QD} = \left(1-Y_{QD}\right)\gamma_{Al_2O_3}^{QD}$ and α is employed to correct the reference radiative lifetime

$$\left\langle \gamma_{Al_2O_3}^{QD^*} \right\rangle = \left[\alpha Y_{QD} + \left(1-Y_{QD}\right)\right]\gamma_{Al_2O_3}^{QD} \tag{S26}$$

C. Analysis of temperature-dependent luminescence lifetimes of the QDs

Analyses of the TRF decay curves were carried out by using multi-exponential curve fitting to the experimental data. Below 50 K, a fast lifetime component in the TRF of the QDs was observed (Figure S2). Since this component has a small steady state contribution, which is

below 2.5% for all samples and temperatures, we ignored that component while fitting the curves. At cryogenic temperatures, this type of behavior for the QDs was first observed by Labeau *et al*. using single CdSe/ZnS QDs.[7] Single QD lifetimes having more than one component including a very fast component were attributed to the relaxation rate from the combined behavior of bright and dark excited states of the QDs. In our study, we observed the similar behavior for the CdSe/ZnS QDs in the ensemble. However, for practical purposes, as this fast component has a weak effect, it is ignored in our analysis.

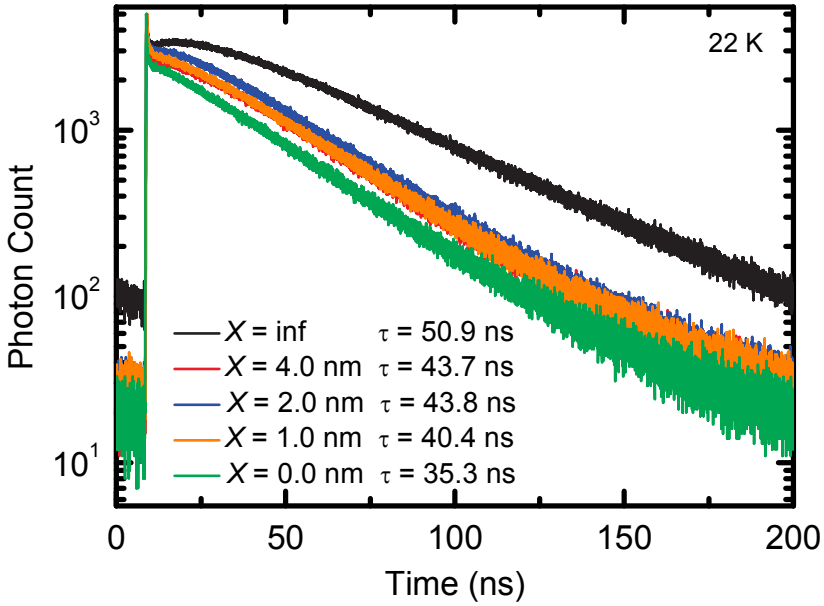

Figure S2. TRF decays of 10-monolayer-equivalent QD film over silicon substrate with 0.0, 1.0, 2.0 and 4.0 nm thick Al_2O_3 separation layer and over sapphire, which were recorded at 22 K.

D. Analysis of inter-dot FRET between the QDs

In this study, we used QDs with low size distribution (<10%). To investigate the effects of inter-dot FRET on the rates, we performed additional TRF measurements using either 10-monolayer-equivalent QD film on top of silicon or highly diluted QDs in solution. For highly

diluted QD solution, inter-FRET is negligible since effective dot-to-dot separation (>50 nm) is much greater than the Förster radius (<10 nm), yet there is difference in the lifetime of the blue- and red-tail emission of the QDs (see Table S0 for highly diluted QD solution cases). This difference is not due to inter-QD FRET, but due to intrinsic difference of the lifetimes of the QDs that are inhomogeneously broadened. In the 10-monolayer-equivalent solid-state films of the QDs, there is an additional difference in the lifetime of the blue- and red-tail emission of the QDs as compared to the lifetime at the peak emission wavelength. Inter-dot FRET is the responsible channel for this extra difference. However, it is so weak that one may neglect its effects. The lifetime difference is only 2.5-fold when compared to the lifetimes of the red- to blue-tail emission considering the intrinsic lifetime difference as measured from the diluted solutions. Here, for the case of far tail emissions +- 40 nm is chosen as compared to the peak emission wavelength. When the experiments are performed at FWHM, the results indicate even smaller lifetime difference of 1.25-fold as shown in Figure S3.

Table S0. Lifetime ratios of the QDs in the emission spectra (lifetimes of the red-tail and blue-tail emission as compared to lifetime at the peak-emission wavelength) when measured for far tail-emission and at FWHM.

At far tails	$\tau_{Red\text{-}tail} / \tau_{Peak}$	$\tau_{Blue\text{-}tail} / \tau_{Peak}$
Highly diluted QD solution	1.2	0.714
Ten-monolayer-equivalent QD film on silicon	1.9	0.455
At FWHM	$\tau_{Red\text{-}tail} / \tau_{Peak}$	$\tau_{Blue\text{-}tail} / \tau_{Peak}$
Highly diluted QD solution	1.4	0.833
Ten-monolayer-equivalent QD film on silicon	1.4	0.666

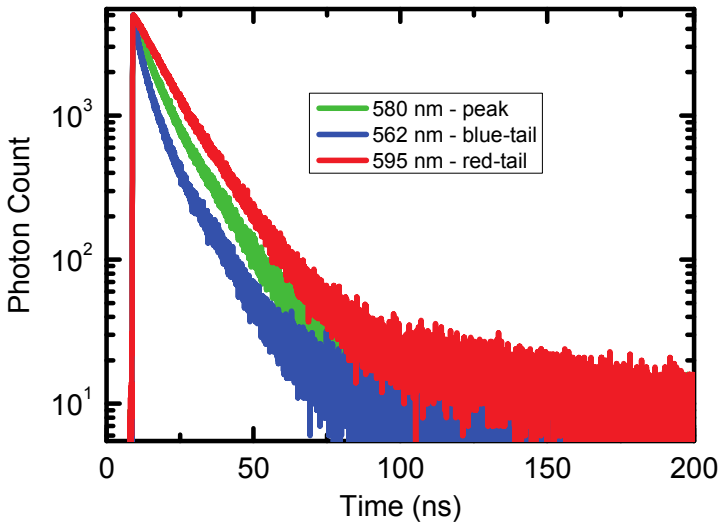

Figure S3. Fluorescence decays of the ten-monolayer-equivalent QDs measured at three different spectral positions (peak, blue- and red-tail) at FWHM.

In the literature, there are several studies related to inter-dot FRET. For example, Crooker et al. utilize a similar QD construct and observe lifetime differences up to an order of magnitude.[8] However, their film thicknesses (up to 1 μm) are totally different than ours (70 nm). In the case of thick QD films, self-absorption effects and cyclic pumping of the smaller bandgap QDs become important. Furthermore, since they use TOPO ligands which are ~1 nm in size, dot-to-dot separation is shorter as compared to our study in which we use HDA ligands (~2 nm in size). All these parameters may cause the differences in lifetimes at various wavelengths.

On the other hand, inter-dot FRET may become dominant with large self spectral overlap and small dot-to-dot distance in between. As recently shown by B. N. Pal *et al.* shell thickness of the QDs strongly affects and thicker shell QDs suppress the inter-dot FRET in dense QD films.[9] Therefore, depending on the material system (core-shell size) and extinction coefficient of the material (self spectral overlap) inter-dot FRET may not be significant.

E. Theoretical Parameters

The theoretical model in our study is clearly based on physical principles and we just employ one fix set of parameters for all the samples differentiated with separation distance and measurement temperature.

a) Dielectric constants and QDs' dipole moment

$$\varepsilon_{SiO_2} = 2.37$$
$$\varepsilon_{Al_2O_3} = 3.10$$
$$\varepsilon_{Ligand} = 1.5$$
$$\varepsilon_{av} = \frac{\varepsilon_{SiO_2} + \varepsilon_{Al_2O_3} + \varepsilon_{Ligand}}{3} = 2.323$$

$$\varepsilon_{CdSeBulk} = 6.2$$
$$\varepsilon_{ZnSBulk} = 8.3$$
$$\varepsilon_{QD} = \frac{\varepsilon_{CdSeBulk} + \varepsilon_{ZnSBulk}}{2} = 7.25$$

$$\varepsilon_{eff\_QD} = \frac{2\varepsilon_{Ligand} + \varepsilon_{QD}}{3}$$

$$d_{exc} = 0.4nm$$

The separation distance from center of the first QD layer to the bulk Si was calculated as follows: $d = l + X + L_l + r$, where X goes from 0 to 4 nm as shown above. Therefore, d = *5.91 nm*, *6.91 nm*, *7.91 nm*, and *9.91 nm*.

The separation distance from center of the second QD layer to the bulk Si was calculated as follows: $d = l + X + L_l + r + D$, where X goes from 0 to 4 nm as shown above. Therefore, d = *12.39 nm*, *13.39 nm*, *14.39 nm*, and *16.39 nm*.

The separation distance from center of the third QD layer to the bulk Si was calculated as follows: $d = l + X + L_l + r + 2D$, where X goes from 0 to 4 nm as shown above. Therefore, d = *18.87 nm*, *19.87 nm*, *20.87 nm*, and *22.87 nm*.

The separation distance from center of the fourth QD layer to the bulk Si was calculated as follows: $d = l + X + L_l + r + 3D$, where X goes from 0 to 4 nm as shown above. Therefore, d = *25.35 nm*, *26.35 nm*, *27.35 nm*, and *29.35 nm*.

The separation distance from center of the fifth QD layer to the bulk Si was calculated as follows: $d = l + X + L_l + r + 4D$, where X goes from 0 to 4 nm as shown above. Therefore, d = *31.83 nm*, *32.83 nm*, *33.83 nm*, and *35.83 nm*.

After the fifth layer the FRET was neglected due to the large separation distance between the QD layer and bulk Si.

b) Factors for temperature-dependent quantum yield

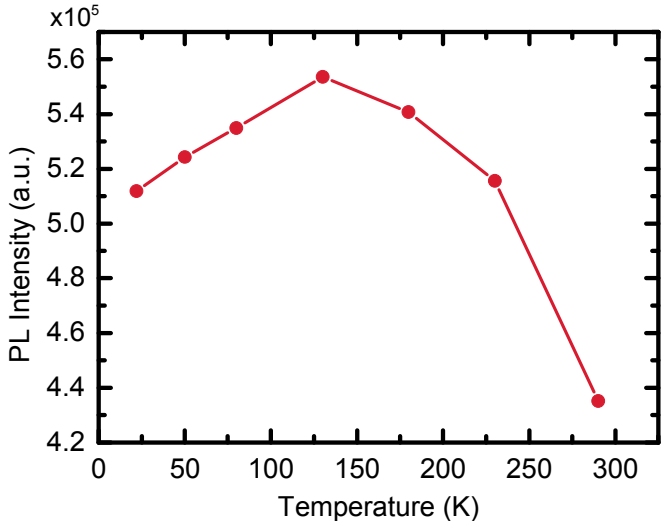

Figure S4. Temperature dependence of PL intensity of the QDs coated on the $Al_2O_3/SiO_2/Si$ and sapphire substrates.

Table S1 shows the experimental QY and gamma ratios with calculated radiative rate ratio compared to room temperature values as obtained by using Eqn. S10.

Table S1. Experimental QY and gamma ratios; and calculated radiative rate ratio for each temperature used in the study.

Temperature (K)	QY ratio	Gamma ratio	Radiative rate Ratio
290	1.000	1.000	1.000

230	1.185	0.940	1.114
180	1.242	0.870	1.081
130	1.272	0.780	0.992
80	1.229	0.610	0.750
50	1.205	0.480	0.578
22	1.176	0.270	0.318

c) Factors for refractive index correction

Table S2 shows the alpha (α) values obtained by using Eqn. S25 and the correction factors obtained by using Eqn. S26.

Table S2. Refractive index correction factors for the QDs' films having QYs of 10%, 25% and 100% and for all the Si samples used in the study.

SiO2/Al2O3 thickness (nm)	Alpha Values	Correction Factors		
		QY=0.1	QY=0.25	QY=1
1.65	1.36688	1.03669	1.09172	1.36688
2.65	1.35475	1.03547	1.08869	1.35475
3.65	1.33658	1.03366	1.08414	1.33658
5.65	1.30311	1.03031	1.07578	1.30311

Table S3 shows the α_i values obtained by using Eqn. S24.

Table S3. Layer-by-layer alpha values for the QDs' films for all the Si samples used in the study.

	Layer-by-layer Alpha Values			
SiO2/Al2O3 thickness (nm)	1. 65	2. 65	3. 65	5. 65
1. layer	2.33428	2.27389	2.19563	2.05356
2.layer	1.94196	1.89957	1.84354	1.7418
3.layer	1.66431	1.63471	1.59458	1.52175

4.layer	1.46853	1.44809	1.41945	1.36755
5.layer	1.33174	1.31791	1.29763	1.26101
6.layer	1.23772	1.22868	1.21452	1.18909
7.layer	1.17479	1.1692	1.15952	1.14228
8.layer	1.13436	1.13121	1.12479	1.11348
9.layer	1.10996	1.10851	1.10441	1.09732
10.layer	1.09669	1.09634	1.09385	1.08965

Table S4 shows the correction factors for each layer for given three different QYs obtained by using Eqn. S26, while substituting α values with α_i for each layer.

Table S4. Layer-by-layer refractive index correction factors for the QDs' films having QYs of 10%, 25% and 100% and for all the Si samples used in the study.

	Layer-by-layer Corrrection Factors for QY = 0.1			
SiO2/Al2O3 thickness (nm)	1. 65	2. 65	3. 65	5. 65
1. layer	1.13343	1.12739	1.11956	1.10536
2.layer	1.0942	1.08996	1.08435	1.07418
3.layer	1.06643	1.06347	1.05946	1.05217
4.layer	1.04685	1.04481	1.04194	1.03675
5.layer	1.03317	1.03179	1.02976	1.0261
6.layer	1.02377	1.02287	1.02145	1.01891
7.layer	1.01748	1.01692	1.01595	1.01423
8.layer	1.01344	1.01312	1.01248	1.01135
9.layer	1.011	1.01085	1.01044	1.00973
10.layer	1.00967	1.00963	1.00939	1.00896
	Layer-by-layer Corrrection Factors for QY = 0.25			
SiO2/Al2O3 thickness (nm)	1. 65	2. 65	3. 65	5. 65
1. layer	1.33357	1.31847	1.29891	1.26339
2.layer	1.23549	1.22489	1.21089	1.18545
3.layer	1.16608	1.15868	1.14865	1.13044
4.layer	1.11713	1.11202	1.10486	1.09189
5.layer	1.08293	1.07948	1.07441	1.06525
6.layer	1.05943	1.05717	1.05363	1.04727
7.layer	1.0437	1.0423	1.03988	1.03557
8.layer	1.03359	1.0328	1.0312	1.02837
9.layer	1.02749	1.02713	1.0261	1.02433
10.layer	1.02417	1.02408	1.02346	1.02241
	Layer-by-layer Corrrection Factors for QY = 1			
SiO2/Al2O3 thickness	1. 65	2. 65	3. 65	5. 65

(nm)				
1. layer	2.33428	2.27389	2.19563	2.05356
2.layer	1.94196	1.89957	1.84354	1.7418
3.layer	1.66431	1.63471	1.59458	1.52175
4.layer	1.46853	1.44809	1.41945	1.36755
5.layer	1.33174	1.31791	1.29763	1.26101
6.layer	1.23772	1.22868	1.21452	1.18909
7.layer	1.17479	1.1692	1.15952	1.14228
8.layer	1.13436	1.13121	1.12479	1.11348
9.layer	1.10996	1.10851	1.10441	1.09732
10.layer	1.09669	1.09634	1.09385	1.08965

d) Temperature-dependent dielectric function of silicon

In the text, we used the following parameters for the temperature-dependent Si dielectric function (Ref. 28 in the main text):

$$\hbar\Omega_{ph,i=1,2} / k_B = 212\ K,\ 670\ K;$$

$$E_{g,j=1,2}(T) = 1.16eV - \frac{\beta \cdot T^2}{T+\gamma}, 2.25eV - \frac{\beta \cdot T^2}{T+\gamma};$$

$$\beta = 7 \cdot 10^{-4}\ \ eV / K,\ \gamma = 1108\ K;$$

$$A_{j=1,2} = 253\ cm^{-1}eV^{-2},\ 3312\ cm^{-1}eV^{-2};$$

$$C_{i=1,2} = 5.5,\ 4.2\ cm^{-1}eV^{-2}.$$

REFERENCES

1. Platzman, P. M.; Wolf, P. A. *Waves and Interactions in Solid State Plasma*, Academic Press, New York, 1973.

2. Govorov, A.O.; J. Lee, J.; Kotov, N.A. Theory of Plasmon-Enhanced Förster Energy Transfer in Optically Excited Semiconductor and Metal Nanoparticles. *Phys. Rev. B* **2007**, *76*, 125308.

3. Hernandez-Martinez P.; Govorov, A.O. Exciton Energy Transfer between Nanoparticles and Nanowires. *Phys. Rev. B* **2008**, *78*, 035314.

4. Palik, E. D. *Handbook of Optical Constant of Solid*, Academic Press, New York, 1985.

5. Novotny, L.; Hecht, B. Principles of Nano-Optics. In *Dipole Emission Near Planar Interfaces*; Cambridge University Press: Cambridge, 2007; pp 335-346.

6. Novotny, L. Allowed and Forbidden Light in Near-Field Optics. I. A Single Dipolar Light Source. *J. Opt. Soc. Am. A* **1997**, *14*, 91-104.

7. Labeau, O.; Tamarat, P.; Lounis, B. Temperature Dependence of the Luminescence Lifetime of Single CdSe/ZnS Quantum Dots. *Phys. Rev. Lett*. **2003**, *90*, 257404.

8. Crooker, S. A.; Hollingsworth, J. A.; Tretiak, S.; Klimov, V. I. Spectrally Resolved Dynamics of Energy Transfer in Quantum-Dot Assemblies: Towards Engineered Energy Flows in Artificial Materials. *Phys. Rev. Lett*. **2002**, *89*, 186802.

9. N. Pal, B.; Ghosh, Y.; Brovelli, S.; Laocharoensuk, R.; Klimov, V. I.; Hollingsworth, J. A. Htoon, H. 'Giant' CdSe/CdS Core/Shell Nanocrystal Quantum Dots As Efficient Electroluminescent Materials: Strong Influence of Shell Thickness on Light-Emitting Diode Performance *Nano Lett*. **2012**, *12*, 331.